Theoretical Mechanics

Volume I

Editor
G. G. Sih

Tsinghua University Press

MESOMECHANICS 2000

Role of Mechanics for Development of Science and Technology

Volume I

Role of Mechanics for Development of Science and Technology

Proceedings of an International Conference of Role of Mechanics for Development of Science and Technology, held at Xi'an Jiaotong University, Xi'an, China, June 13-16, 2000

Edited by

G.C. Sih

Department of Mechanical Engineering and Mechanics,
Lehigh University, Bethlehem, Pennsylvania, USA

Volume I

Tsinghua University Press
Beijing, China

MESOMECHANICS 2000

Proceedings of the Third International Conference for Mesomechanics

Xi'an, P.R. China

Editor: G.C. Sih

Tsinghua University Press

Beijing 100084, P.R. China

Tsinghua

ISBN 7-302-00979-1/O • 231 Set of 2 Volumes

Antisymmetric stress component associated with polycrystal deformation and fracture of mesovolumes

I.Y. Smolin [a], P.V. Makarov [b], Y.P. Stefanov [a], D.V. Shmick [b], I.V. Savlevich [b]

[a] *Institute of Strength Physics and Materials Science, Siberian Branch of Russian Academy of Sciences, 2/1 Academicheskii pr., Tomsk, 634021, Russia*

[b] *Tomsk State University, 36 pr. Lenina, Tomsk, 634050, Russia*

Abstract

Plastic deformation and fracture in mesovolumes of polycrystalline materials are investigated for the case of dynamic loading. Heterogeneity of material structure is accounted for the different mechanical properties of grains and grain boundaries. Accounted for is the non-symmetric force stress arising from plastic deformation in the grains with a limited number of activated slip systems. Formation of shear bands and rotation of meso-fragments are modelled using mesovolumes of polycrystalline material under dynamic loading. Examples are given for the development of mesocracks leading to spall fracture under shock wave loading.

1. Introduction

Localized plastic deformation and shear band formation have received little attention in the literature. They are influenced by the material internal structure, property and loading. Physical mesomechanics has been used [1,2] to analyze the plastic deformation and fracture process at three scale levels. This involves generation and evolution of microheterogeneous plastic deformation in the form of slip lines, microscale shear bands etc. When dissipation is suppressed, the dominant process shifts to a higher scale level, say mesolevel. Strain localization at the macrolevel is usually completed when the specimen fails. Fracture is considered to be the final stage of plastic deformation. Nucleation of microcracks occurs when energy dissipation terminates at the microlevel except for discontinuity. Similarly, mesocracks could open along the mesobands under similar conditions. This is caused by mesoblock rotation.

Force stress can become non-symmetric [3] in grains where only one or two slip systems are activated. Antisymmetric part of the force has been considered in [4] without calculating couple stress and independent rotations that are required in micropolar theory. In particular, antisymmetric stress has been defined as

$$\sigma_{12}^{A} = -\sigma_{21}^{A} = \alpha \varepsilon_{eff}^{pl} \tag{1}$$

$$\sigma_{12}^{A} = -\sigma_{21}^{A} = \beta \left| \mathrm{grad} \left(\varepsilon_{eff}^{pl} \right) \right| \tag{2}$$

Calculations for slow-rate tension and compression have shown that such behavior is similar to the deformation of single crystals with one activated slip system [4]. In what follows, numerical analyses will be made for localized plastic deformation involving non-symmetric force stress and spall fracture at the mesolevel.

2. Localized deformation and rotation at mesolevel

A mesovolume made of Al alloy containing a large number of grains has been selected for the numerical analysis. Different yield strength and α (or β) parameters in eqs. (1) and (2) are used to define the antisymmetric stress for different grains. Variations of the bright to dark intensity in Fig. 1(a) correspond to different intensities of the parameters. Plane strain is assumed and symmetry boundary conditions are imposed on sides of the mesovolume parallel to the y-axis. Particle velocities at the top of mesovolume correspond to a plane shock wave with intensity 3 GPa. They are specified for the appropriate grid nodes for the calculation. The bottom side of the mesovolume is assumed to be stress free. A finite difference method [5] is used for an elastic perfectly plastic material that yields according to the von Mises criterion.

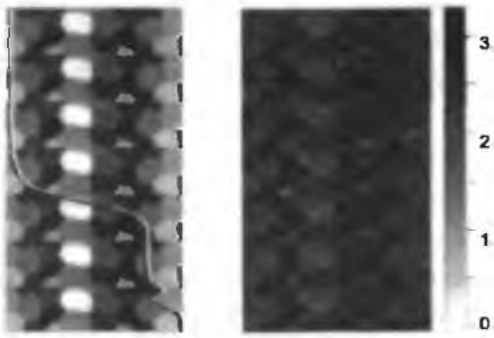

(a) Mesovolume (b) ε^{pl} (%)

Fig. 1 Map of mesovolume accumulated plastic deformation

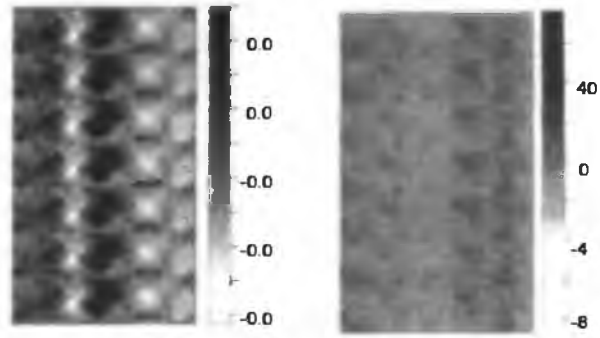

(a) σ_{xy} (GPa) (b) $\dot{\omega}$ (μs^{-1})

Fig. 2 Shear stress and rotation rate

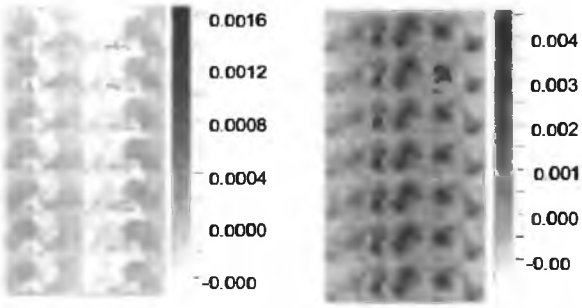

(a) σ^{A}_{xy} (GPa) –eq. (1) (b) σ^{A}_{xy} (GPa) –eq. (2)

Fig. 3 Antisymmetric stress in mesovolume for two models

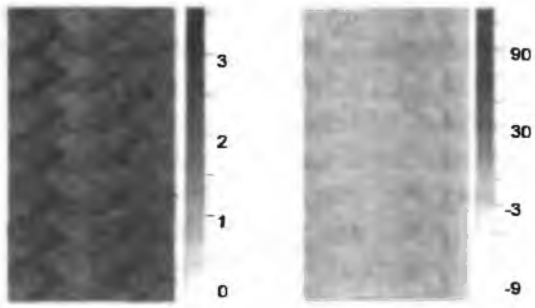

(a) ε^{pl} (%) (b) $\dot{\omega}$ (μs^{-1})

Fig. 4 Effective plastic deformation and rotation rate for larger antisymmetric stress

Stress, effective plastic strain ε^{pl}, rotation rate $\dot{\omega}$, and particle-velocities v are obtained. In contrast to the experiment where data are measured after waves are released and stress relaxation is complete. The calculation starts with the initiation of strain localization prior to the release waves. Fig. 1(b) shows the distribution of plastic strain. Position of the shock wave front is shown by the curve in Fig. 1(a). Distribution of shear stresses σ_{xy} and rotation rate $\dot{\omega}$ are displayed in Figs. 2(a) and 2(b), respectively. The results for the two models are similar for the same α and β. Distribution of the antisymmetric stresses in Figs. 3(a) and 3(b), however, are different. Although the effective plastic strain in Fig. 4(a) is similar to that in Fig. 1(b), significant change is observed for $\dot{\omega}$ in Fig. 4(b). When α is ten times larger on the average, the antisymmetric stresses are five times larger.

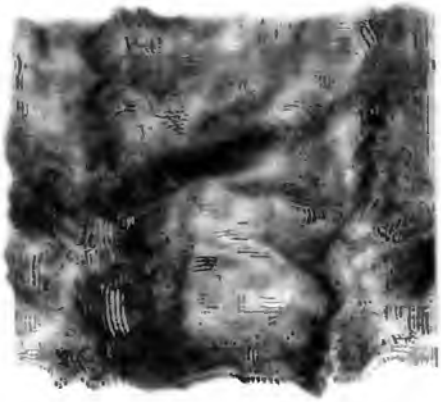

Fig. 5 Velocity vector field for difference of homogeneous and heterogeneous media

Fig. 6 mesovolume structure and loading scheme

Different properties of structural elements result in non-uniform stress-strain state that is reflected in the velocity field [6]. Fig. 5 shows the difference of particle velocities for the heterogeneous and homogeneous material. It pertains to the region outlined by the white dash line in Fig. 6. The particle velocity field shows the effect of rotation of the grains at the shock wave front. Fracture of the specimen may occur along the boundaries of blocks that are visible in Fig. 5.

Different pattern is observed for specimens under tension and compression. Figs. 7(a) and 7(b) refer to mesovolume with a great numbers of grains. Three groups 1, 2 and 3 can be identified. Spins $\pm\alpha$ are varied for individual grains with magnitude close to the average of the group. Groups 1 and 2 refer to $+\alpha$ and group 3 to $-\alpha$. They are chosen such that the rotation angles correlate with the experimental data for individual fragments from fraction of a degree up to several degrees [7, 8]. Under tension, the plastic deformation is localized and grains tend to rotate as a whole. Computed pattern of plastic deformation and rotation fields can be found in Figs. (8) to (10) with shear bands propagating close to the directions of principal tangential stresses. Note that the shear bands and interfaces of the rotated blocks do not match exactly at the boundaries of the three groups.

More specifically, Figs. 8(a) and 8(b) give the isolines of plastic deformation for the grains in Figs. 7(a) and 7(b), respectively. Note that group 3 in Fig. 7(a) is separated into two parts as shown in Fig. 8(a). The mesovolume in Fig. 7(b) is also separated by shear band into two parts, Fig. 8(b). These computed results agree qualitatively with the experimental data [1,9-11] where different degrees of deformation domains are formed and then rotate. The different grain groups could rotate in opposite directions or the same direction with different velocities that could result in cracking [1,10]. Isolines corresponding to "–" (anticlockwise) and "+" (clock wise) rotations can be found in Figs. 9 and 10, respectively, for the grain groups in Figs. 7(a) and 7(b).

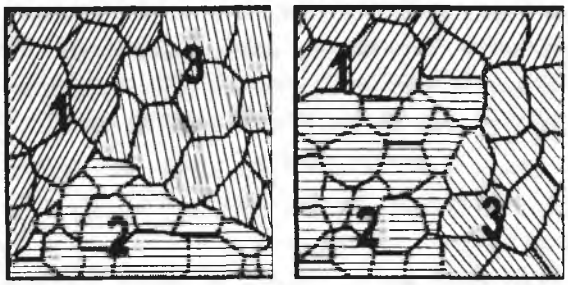

(a) First combination (b) Second combination

Fig. 7 Initial structure of polycrystalline materials with $\pm\alpha$ spines

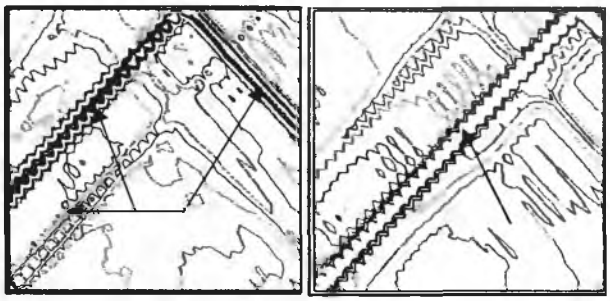

(a) For Fig. 7(a) (b) For Fig. 7(b)

Fig. 8 Isolines of plastic deformation field

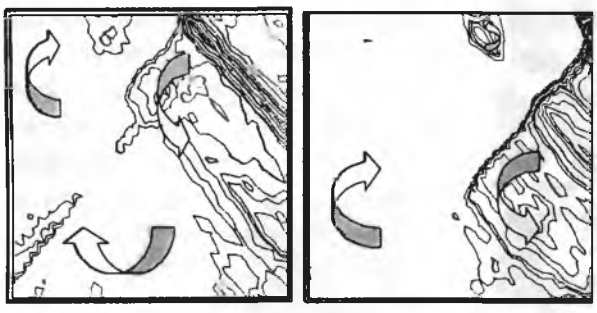

(a) For Fig. 7(a) (b) For Fig. 7(b)

Fig. 9 Display of isolines for "–" rotations with step of 2×10^{-4} radian

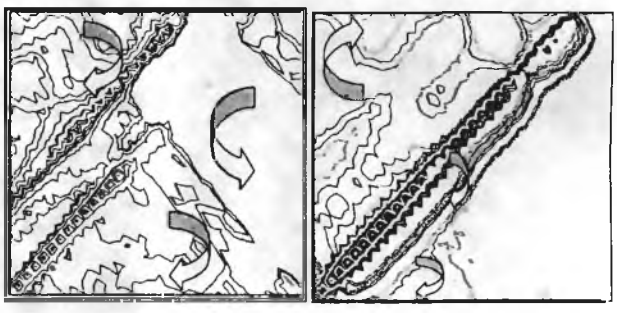

(a) For Fig. 7(a) (b) For Fig. 7(b)

Fig. 10 Display of isolines for "+" rotations

3. Fragmentation and spall fracture

Spall fracture at the mesolevel will be studied involving the development of cracks in a polycrystalline steel under shock wave loading. Mesovolume is introduced with grains having different yield and strength properties in the calculations. Moreover, intergranular layer is introduced to account for grain boundary effects. A node splitting algorithm is used for modelling the formation and opening of cracks. Criteria for instantaneous spall and damage accumulation of the type

$$\int_{t_o}^{t_{fr}} (\sigma_{eff} - \sigma_0)^{\lambda} \Phi^{-1} dt = 1 \qquad (3)$$

are adopted.

Different patterns of crack distribution in Fig. 10(a) are given in Figs. (11) and (12). Spalling cracks are generated in the region of tensile wave formation after reflection of shock wave from the back free surface. Their arrangement and orientation are determined by the pulse intensity and its duration in addition to strength of the individual grains and intergranular layer. Onset of spalling is determined by the different critical stresses. When the

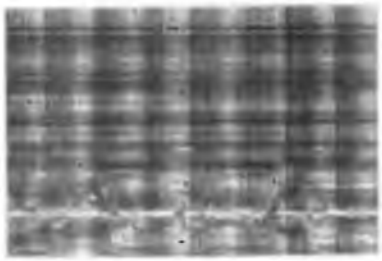

(a) Fracture in narrow region

(b) Fracture across grains

(c) Wide spread fracture

Fig. 11 Fracture pattern in mesovolume at spalling using an instantaneous fracture criterion

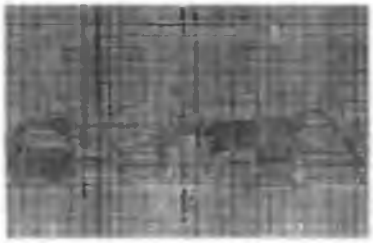

(a) Early damage

(b) More severe damage (later time)

(c) Grain boundary details

Fig. 12 Crack distributions at different time moments with damage accumulation

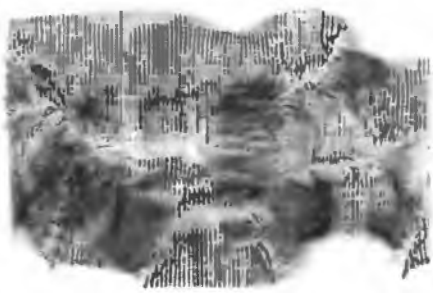

(a) Earlier time

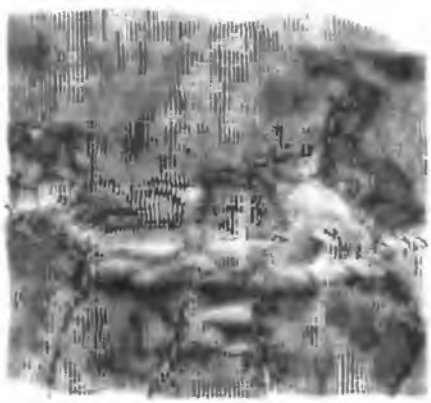

(b) Later time

Fig. 13 Velocity fields at different times for material under fracture

critical stress σ_0 is high (or shock wave amplitude is low), the corresponding spallation pattern are shown in Figs. 11(a) and (b). Fracture is located in a narrow region. Material separation occurs after formation of the tensile pulse. Since the material unloads after separation, tensile stresses sufficient to cause fracture tend to be confined in a narrow zone. If the critical stress σ_0 is low, the region of fracture is more wide spread, Fig. 11(c). This is associated with the onset of crack formation in a material taking place prior to complete

generation of the tensile stress pulse. A propagating tensile wave is capable of inducing multiple fracture over a region before the wave energy is exhausted. That is repeated spallation can take place. Many cracks with different orientations could merged together to form a complex-shaped macrocrack. When considering damage accumulation, the fracture zone size may be even wider than that predicted instantaneously. Total destruction of the material then takes place in the zones shown in Figs. 12(a) and 12(b) for two time moments. Fig. 12(c) shows the details at the grain boundaries. Figs. 13(a) and 13(b) display the velocity fields for two different times. These patterns reflect crack generation and growth.

4. Conclusions

The influence of antisymmetric stress on stress and strain state and strain localization in front of the shock wave may be significant if the magnitude of antisymmetric stress is more than half of the symmetric shear stress. When local properties are considered at the mesolevel, the process of multiple cracking can be described. Difference in the yield and strength properties could yield a variety of crack distribution in the mesovolumes.

References

[1] V.E. Panin, Foundations of physical mesomechanics, *Phys. mesomech.*, 1, 5–20 (1998).

[2] P.V. Makarov, Physical mesomechanics approach in simulation of deformation and fracture processes, *Phys. mesomech.*, 1, 57–76 (1998).

[3] P.V. Makarov, O.I. Cherepanov, V.N. Demidov, Mathematical model of elastoplastic deformation of a mesovolume of material with a limited number of slip systems, *Izv. Vyssh. Uchebn. Zav.*, 11, 26–57 (1995) (in Russian).

[4] P.V. Makarov, Character of localized deformation and fracture of solids at mesolevel, *Int. Conf Mesomechanics-2000*, in: George C. Sih (ed.), Xi'an, China, 2000, (Tsinghua Univ. Press, 2000).

[5] M.L. Wilkins, Calculation of elastic-plastic flow, *Methods in Computational Physics*, in: B. Alder, S. Fernbach, M. Rotenberg (eds.), (Academic Press, Vol. 3, 211–263, 1964).

[6] V.E. Panin, P.V. Makarov, I.Y. Smolin, Physical mesomechanics of materials and its impact on shock chemistry, *Proc. USA-Russian Workshop "Shock-Induced Chemical Processing"*, St. Petersberg, Russia, 1996, 88-92 (1997).

[7] V.V. Rybin, *High Plastic Strains and Fracture of Metals*, (Metallurgiya, 1986), (in Russian).

[8] *Physical Mesomechanics of Heterogeneous Media and Computer-Aided Design of Materials*, in: V.E. Panin (ed.), (Cambridge International Science Publishing, 1998).

[9] V.E. Panin, Physical foundations of mesomechanics of plastic deformation and fracture of solids, *Physical Mesomechanics and Computer-Aided Design of Materials*, (Nauka, Vol. 1, 7-49, 1995), (in Russian).

[10] V.E. Panin, A.D. Korotaev, P.V. Makarov, V.M. Kuznetsov, Physical Mesomechanics of Materials, *Izv. Vyssh. Uchebn. Zav., Fiz.*, 9, 8-36, (1998), (in Russian).

[11] V.E. Panin, Modern problems of plasticity and strength of solids, *Izv. Vyssh. Uchebn. Zav.*, Fiz., 1, 7–34 (1998), (in Russian).